REDUCING THERMAL CONDUCTIVITY OF THERMAL BARRIER COATING MATERIALS WITH DOPING

Dongmei Wang and Xiao Huang

Carleton University, Ottawa, Ontario, Canada

Abstract

Metal oxides of different valence, ionic radius and mass were incorporated into yttria partially stabilized zirconia (YSZ) in order to investigate the thermal conductivity changes as a result of co-doping. A Mechanical alloying process was used to produce powder blends which were subsequently sintered at 1500°C for 120 hours. The sintered samples were then subjected to detailed examination to determine their thermal conductivities. It was found that, in general, the trivalent oxides Yb_2O_3, Sc_2O_3 and Cr_2O_3, exhibited the most significant effect on reducing the thermal conductivity of 7YSZ (7 wt%Y_2O_3-ZrO_2). This trend was followed by the pentavalent co-doping oxides of Nb_2O_5 and Ta_2O_5 whereas the tetravalent CeO_2 co-doped 7YSZ showed a lesser effect.

1. Introduction

Thermal barrier coatings (TBCs) play an important role in protecting substrate components from reaching excessive temperatures. Among a number of engineering ceramic materials, zirconium oxide, ZrO_2 (zirconia), exhibits a lower intrinsic thermal conductivity and superior fracture toughness. Accordingly, the development of thermal barrier coatings in the past several decades has focused primarily on zirconia-based ceramic materials. Pure zirconia is not used in structural applications due to the destructive phase transformation from the high temperature tetragonal (*t*) phase to room temperature monoclinic (*m*) phase. The addition of metal oxides, or so-called dopants, to the ZrO_2 matrix can delay this phase transformation, thereby preventing failure. When dopants with a cation valence less than +4 are added to zirconia to replace Zr^{4+}, oxygen vacancies are formed in order to maintain the charge balance [1] and as a result, the high temperature cubic (*c*) or tetragonal phase (*t*) is stabilized by the presence of oxygen vacancies. The material of choice for thermal barrier application has been 7 wt.% yttrium oxide Y_2O_3 (yttria) partially stabilized ZrO_2 (7YSZ) due to its stable microstructure (meta-stable *t'* phase when cooling directly from the single cubic (*c*) phase region), low thermal conductivity, compatibility with Ni-based alloys and MCrAlY bond coat systems, higher toughness and phase stability up to 1200°C [2]. However, prolonged exposure to temperatures above 1200°C results in phase separation from $t' \rightarrow t+c$, and $t \rightarrow m$ occurs upon cooling to room temperature.

Despite the widespread application of 7YSZ, the continued demand for TBC materials with lower thermal conductivity at service temperatures and increased phase stability requires further research into newer materials or dopants for ZrO_2. Dopants play a significant role in modifying the thermal conductivity of ceramic materials. According to thermal conductivity theory, the scattering effect is associated with the type of point defect (oxygen vacancy or substitutional defects) and the characteristics of the substitutional cations (mass, ionic radius, valence) [3,4].

The vacancies formed in ZrO_2 due to doping with lower valence cations, such as Y^{3+}, Sc^{3+} and Yb^{3+}, strongly scatter phonons by virtue of both missing mass and inter-atomic linkage [5-7] and result in a decrease in thermal conductivity [8]. The substitutional cations, replacing the host Zr^{4+} cations, also increase scattering of phonons and further reduce the thermal conductivity. It has been reported that the measured thermal conductivities of zirconia-based bulk materials and coatings decrease with increasing yttria content [9]. Additions of other transition metal oxides and rare earth oxides to YSZ have also shown a thermal conductivity reduction effect [5,6].

In addition to the valence effect, the ionic mass and radius of the dopant ions were found to play certain roles in altering the thermal conductivity of zirconia when co-doped with Y_2O_3, Ta_2O_5 and Nb_2O_5 [10]. Additions of dopants with high atomic mass or larger ionic radius seemed to provide more effective scattering [4]. These observations have been experimentally validated in a binary zirconia system doped with trivalent Sc^{3+}, Yb^{3+} or Y^{3+}, where the thermal conductivity of zirconia decreased with the increase in ionic radius of the dopant cations [7,11]. Reduction in thermal conductivity was also found to be associated with larger atomic masses of dopants in a zirconia system doped with Nd_2O_3, Gd_2O_3 Er_2O_3 and Yb_2O_3 [6].

A series of co-doped 7YSZ samples were investigated in this study in order to understand how the bulk material thermal conductivity changes as a result of co-doping. Six different co-dopants were selected with varying oxygen vacancies, ionic mass and radius. Bulk ceramic samples were fabricated using mechanical alloying and furnace sintering.

2. Experimental Procedures

2.1 Materials

Table 1 lists the co-dopant oxides used in this study. Pentavalent oxides Ta_2O_5 and Nb_2O_5 were selected to examine the effect of co-doping while eliminating oxygen vacancies present in 7YSZ. To investigate the effect of additional oxygen vacancies and co-dopant cations at the same time, trivalent oxides Sc_2O_3, Cr_2O_3 and Yb_2O_3 were incorporated into 7YSZ. Lastly tetravalent CeO_2 was added to 7YSZ to examine the effect of co-dopant without changing oxygen vacancies.

Table 1 Compositions of the dopant cations in doped 7YSZ systems.

Sample ID	Co-dopant	Atomic mass (amu)	Ionic radius	Co-dopant cations	Y^{3+}
7YSZ	Y_2O_3	88.91	0.089 nm	-	7.6 mol%
7TaYSZ	Ta_2O_5	180.95	0.068 nm	7.05 mol%	7.06 mol%
7NbYSZ	Nb_2O_5	92.91	0.069 nm	7.05 mol%	7.06 mol%
5CrYSZ	Cr_2O_3	52.00	0.063 nm	4.71 mol%	7.23 mol%
5ScYSZ	Sc_2O_3	44.96	0.072 nm	4.71 mol%	7.23 mol%
5YbYSZ	Yb_2O_3	173.04	0.086 nm	4.71 mol%	7.23 mol%
5CeYSZ	CeO_2	140.11	0.092 nm	4.71 mol%	7.23 mol%
(Host)	ZrO_2	91.22	0.079 nm	-	-

The amount of pentavalent co-dopants was calculated to be equal to the mol% of Y^{3+} (to remove the oxygen vacancies in 7YSZ). The trivalent and tetravalent co-dopants were added to 7YSZ to achieve 12 mol % of total dopant cation concentration in the ZrO_2 substrate. The sample ID was determined based on the rounded mol% of co-dopant cations present in 7YSZ. High purity crystalline 7YSZ was purchased from Praxair Surface Technology (US). Ta_2O_5, Sc_2O_3, CeO_2 and Yb_2O_3 were obtained from Metall Rare Earth Limited (China). Cr_2O_3 and Nb_2O_5 were from Sigma-Aldrich (US). The purity of all co-dopant materials was greater than 99.9%.

2.2 Fabrication of Co-Doped Bulk Materials

For each composition given in Table 1, a powder mixture was blended and mechanically alloyed using a ball-milling machine for 50 hours. After ball milling, green compact disks of 15 mm diameter were made using cylindrical die sets and uniaxially pressing at 200 MPa. Sintering at 1500°C for 120 hrs was used to consolidate the material. After sintering, the samples were furnace cooled at ~ 5^{o}C/min from 1500°C to 700°C followed by air cooling.

2.3 Characterization Techniques

Microstructure characterization was conducted using a scanning electron microscope (SEM). Thermal conductivity λ of the sintered samples was evaluated using the following relationship [12]:

$$\lambda = \alpha \cdot C_P \cdot \rho \tag{1}$$

Where C_p is the specific heat capacity (J/kg·K), α is the thermal diffusivity (m^2/s), and ρ is the bulk density (kg/m^3).

The specific heat capacity C_p was measured using a DSC (differential scanning calorimetry). The thermal diffusivity α was measured using a laser flash technique (Industrial Materials Institute, Montreal, Canada). The basic principle of the laser flash measurement involved rapid heating of one side of the specimen using a pulsed laser and measuring the temperature rise on the opposite side [13]. The time measured for the heat to travel through the sample and cause the temperature to rise on the rear face was used to calculate the diffusivity.

The bulk density was measured using Archimedes' method [14]. As the thermal conductivities measured from materials with porosities are lower than those of fully sintered samples, a correction factor needs to be introduced. Assuming all the pores in the sintered samples are spherical, the thermal conductivity of dense, porosity-free material λ_{dense} can be evaluated using the following equation [15]:

$$\frac{\lambda_{porous}}{\lambda_{dense}} = 1 - \frac{4P}{3} \tag{2}$$

Where P is the volume fraction of pores inside the sintered sample obtained from image analysis and λ_{porous} is the measured thermal conductivity of the material containing porosity.

3. Results

3.1 Microstructure

The microstructures of sintered materials were examined using SEM. For comparison purposes, the microstructure of 7YSZ was also examined, as shown in Figure 1. From the observation of the sintered samples, 7NbYSZ and 5CeYSZ exhibited strong powder particle bonding and consolidation after 120 hour sintering at 1500°C. This was indicated by the smoother surface and well-defined grain structure on the as-sintered surface. Samples with compositions of 7YSZ, 7TaYSZ and 5CrYSZ showed adequate sintering but some surface particles were not fully bonded as compared to that of 7NbYSZ and 5CeYSZ. Slightly porous surface morphology was observed for both 5ScYSZ and 5YbYSZ.

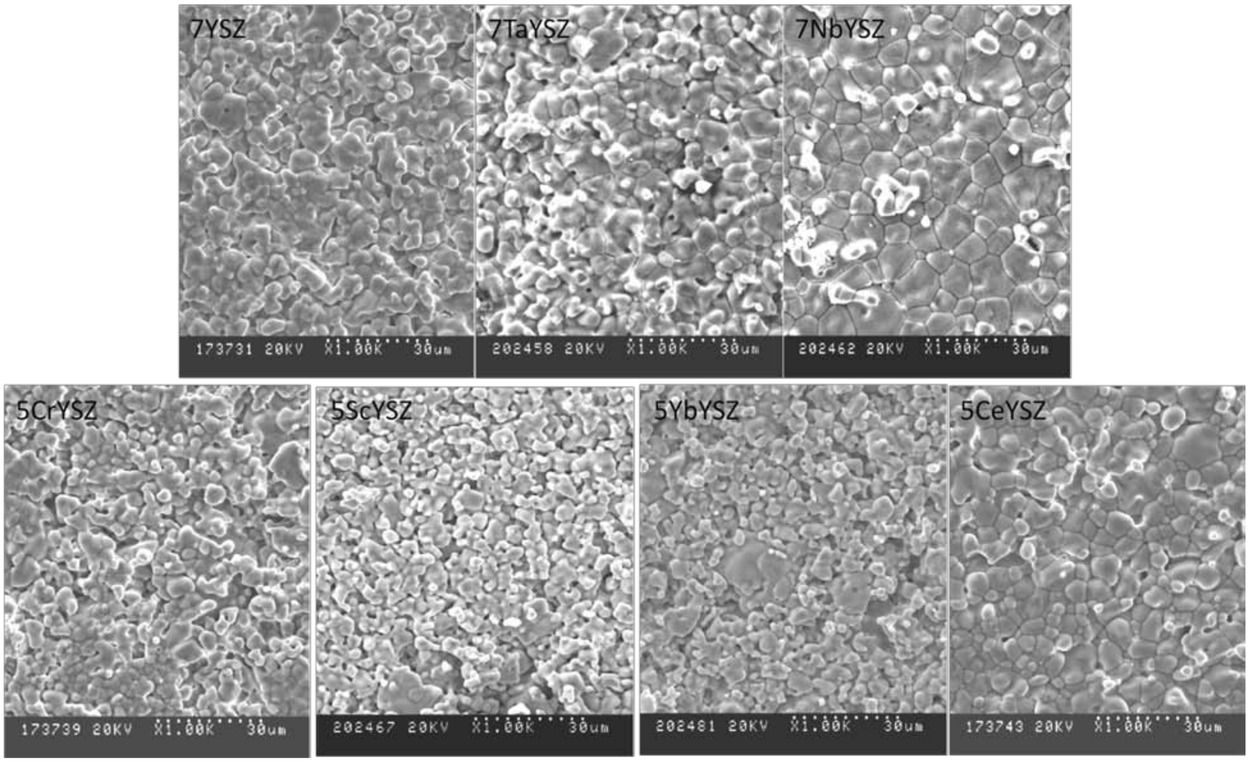

Figure 1 Microstructure of sintered samples.

3.2 Bulk density and volume fraction of porosity

The measured bulk densities of co-doped samples are summarized in Table 2 along with theoretical densities included as reference. The porosity measurement results (volume percentages of pores measured using image analysis) are also given in Table 2. The information shown in Table 2 indicates that the sintered 7NbYSZ and 5CeYSZ samples reached as high as about 95% of the fully sintered material and exhibited good sinterability while other samples (particular trivalent oxide co-doped 5ScYSZ and 5YbYSZ) had lower relative densities of 86-87%, indicating their sintering resistance.

Table 2 Measured density and volume fraction of porosity.

Sample ID	Theoretical density (g/cm^3)	Measured density (g/cm^3)	Porosity (vol.%)
7YSZ	6.06	5.57	13.19
7TaYSZ	6.12	5.82	8.81
7NbYSZ	6.02	5.70	4.68
5CrYSZ	6.01	5.44	12.13
5ScYSZ	5.96	5.30	13.36
5YbYSZ	6.22	5.66	14.12
5CeYSZ	6.14	5.92	5.30

3.3 Specific heat capacity

The specific heat capacity of each doped material was calculated from the measurements of heat flux for the baseline (pure metals), a standard sapphire and the corresponding sample. Table 3 displays the results in heat capacity values for each sample at 100°C, 600°C and 800°C. An increasing trend in specific heat capacity value was observed with rising temperatures.

Table 3 Measured specific heat capacity values.

Sample ID	Specific heat Cp (J/kg·K)		
	100°C	600°C	800°C
7YSZ	491.70	1076.31	1153.54
7TaYSZ	438.52	739.56	920.38
7NbYSZ	554.55	819.71	864.48
5CrYSZ	525.40	975.46	896.04
5ScYSZ	496.51	918.26	940.45
5YbYSZ	490.14	557.58	533.51
5CeYSZ	565.39	984.91	948.75

3.4 Thermal diffusivity

The thermal diffusivities of the samples were measured three times at each of the three different temperatures. The average values along with standard deviations are shown in Table 4. The thermal diffusivities of all samples decreased with increasing temperature; this trend is consistent with the literature data. Extremely low thermal diffusivities of 7TaYSZ and 7NbYSZ were observed at elevated temperatures. Since powder-like structures were found for these two samples after testing, it is believed that the phase transformation (*t*↔*m*) occurred during testing causing specimens to crack into powders.

Table 4 Thermal diffusivities (α) and standard deviations at different temperatures.

Sample ID	$22^{o}C$	$600^{o}C$	$800^{o}C$
	$\alpha\ (10^{-7}\cdot m^2/s)$	$\alpha\ (10^{-7}\cdot m^2/s)$	$\alpha\ (10^{-7}\cdot m^2/s)$
7YSZ	12.00 ± 0.14	5.45 ± 0.01	5.78 ± 0.01
3.9TaYSZ	8.37 ± 0.05	1.52 ± 0.01	1.10 ± 0.03
3.9NbYSZ	9.29 ± 0.01	1.71 ± 0.01	1.49 ± 0.01
5CrYSZ	7.93 ± 0.03	5.27 ± 0.02	5.75 ± 0.01
5ScYSZ	7.60 ± 0.07	6.28 ± 0.10	5.98 ± 0.05
5YbYSZ	6.53 ± 0.09	5.18 ± 0.02	4.96 ± 0.02
5CeYSZ	9.65 ± 0.04	6.81 ± 0.09	6.47 ± 0.02

3.5 Thermal conductivity

Thermal conductivities were obtained using equation (1). The values of the measured density (ρ), specific heat (Cp), and thermal diffusivity (α) are from Table 2, Table 3 and Table 4, respectively. The specific heat capacity measured at 100°C was used to calculate the room temperature thermal conductivity due to the inability of DSC to measure room temperature properties. The porosity values (Table 2) were used to correct the thermal conductivity λ_{porous} to that of the fully dense material λ_{dense} using equation (2).

As shown in Table 5, all co-doped samples examined in this study had lower thermal conductivities than 7YSZ, illustrating the effect of co-doping. In particular, 7TaYSZ and 7NbYSZ exhibited lower thermal conductivities than 7YSZ even though the vacancies that existed in the original 7YSZ were annihilated by the addition of Ta^{5+} and Nb^{5+}. It is evident that the introduction of substitutional point defects is able to create strong phonon scattering centers due to the differences in ionic radius and mass between the co-dopant cations and the host cation Zr^{4+}. Ta^{5+} (m_{Ta} = 180.95 g/mol) with higher atomic mass showed a stronger effect in lowering the thermal conductivity than Nb^{5+} (m_{Nb} = 92.91 g/mol) at room temperature. The smaller ionic sizes of Ta^{5+} and Nb^{5+} (than Zr^{4+}) may also have played a role in modifying the thermal conductivities of the co-doped samples. At elevated temperatures (Figure 2), further reduction in thermal conductivity for 7TaYSZ and 7NbYSZ was also observed. However, 7TaYSZ and 7NbYSZ had similar thermal conductivities at these temperatures.

For trivalent oxide co-doped samples (5CrYSZ, 5ScYSZ and 5YbYSZ), a more significant reduction in thermal conductivities was observed. This can be attributed to the addition of M^{3+} to 7YSZ in creating more oxygen vacancies in addition to substitutional defects and increasing the numbers of both types of phonon scattering centers. Yb^{3+}, with the highest atomic mass (173.04 g/mol), had an even greater impact on the thermal conductivity at elevated temperature, giving 42% and 50% reductions in thermal conductivities at room temperature and 800°C, respectively.

Table 5 Thermal conductivities of co-doped materials at room temperature.

Sample ID	Specific heat capacity (J/kg.K) (100°C)	Thermal diffusivity α (m^2/s) (22°C)	λ_{dense} (W/m·K)	% of Reduction (7YSZ as baseline)
7YSZ	491.70	12	3.99	-
7TaYSZ	438.52	8.37	2.57	36%
7NbYSZ	554.55	9.29	3.13	22%
5CrYSZ	525.40	7.93	2.70	32%
5ScYSZ	496.51	7.6	2.35	41%
5YbYSZ	490.14	6.53	2.30	42%
5CeYSZ	565.39	9.65	3.23	19%

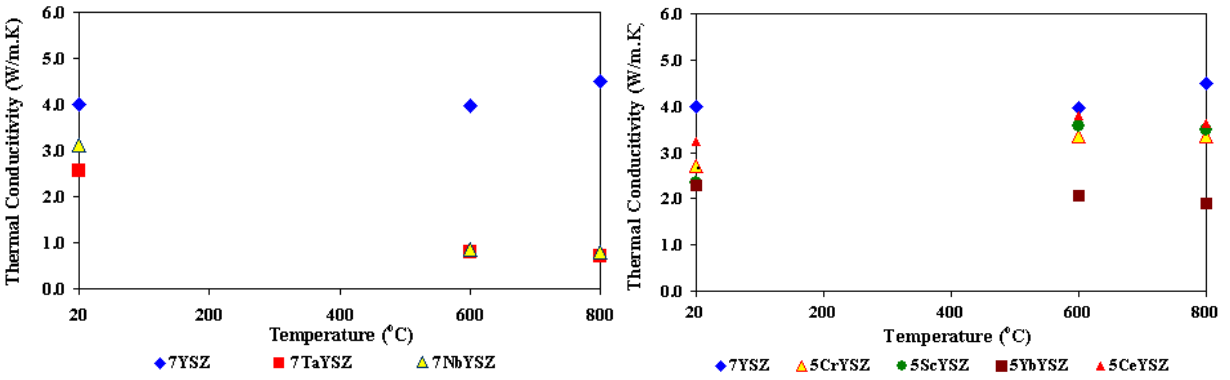

(a) (b)

Figure 2 Thermal conductivity as a function of temperature. (a) 7YSZ, 7TaYSZ and 7NbYSZ. (b) 7YSZ, 5CrYSZ, 5ScYSZ, 5YbYSZ and 5CeYSZ.

The addition of tetravalent CeO_2 also reduced the thermal conductivity of the material. This can be attributed to the addition of substitutional lattice defects. While its effect was not as significant as that of the trivalent dopants observed in this study, the addition of a tetravalent oxide has other advantages such as enhancing fracture toughness [16]. Further study is currently being undertaken to examine the effect of TiO_2 addition on the thermal and mechanical properties of co-doped 7YSZ.

4. Conclusions

The thermal conductivities of various co-doped 7YSZ bulk materials were evaluated by measuring the density, specific heat capacity and thermal diffusivity. Based on the results, it was found that the addition of the six co-dopants to 7SYZ resulted in substantial thermal conductivity reduction. In particular, the trivalent oxides Yb_2O_3 and Sc_2O_3 exhibited the most significant effect on reducing the thermal conductivity of 7YSZ. This was followed by pentavalent co-doping oxides of Nb_2O_5 and Ta_2O_5 while the tetravalent CeO_2 co-doped 7YSZ showed the least change. In selecting potential dopants or co-dopants, other properties such compositional compatibility, modulus of elasticity and fracture toughness must also be taken into consideration.

5. Acknowledgements

The authors thank NSERC (Natural Science and Engineering Research Council) for providing a discovery grant to support this research. We also thank Mr. Mario Lamontagne for helping with the laser flash test.

6. References

[1] A. Dwivedi and A. N. Cormack, "A computer simulation study of the defect structure of calcia-stabilised zirconia", *Phil. Mag.* A, Vol. 61, 1990, pp.1-22.
[2] S. Stecura, S., "Optimization of the NiCrAl-Y/ZrO_2-Y_2O_3 thermal barrier system", NASA Tech. Memo No. 86905, 1985.
[3] D. Zhu, Y. Chan and R. A. Miller, "Defect clustering and nano-phase structure characterization of multi-component rare earth oxide doped zirconia -yttria thermal barrier coatings", *American Ceramic Society*, Vol. 23, 2002, pp.457-468.
[4] P. G. Klemens, "*Thermal Conductivity*", ed. K.E. Wilkes, Technomics, Lancaster (PA), Vol.23, 1996, pp.209-220.
[5] Y. A. Tamarin, E. B. Kachanov and S. V. Zherzdev, "Thermophysical properties of ceramic layers in EB-TBC", 4th Inst. Symposium, *High Temperature Corrosion*, *Mater. Sci. Forum*, Vols. 251-254, 1997, pp.949-956.
[6] D. S. Rickerby, European Patent, 1998, EP 0825271 A1.
[7] U. Schulz, C. Leyens, K. Fritscher, M. Peters, B. Saruhan-Brings, O. Lavigne, J-M. Dorvaux, M. Poulain, R. Mevrel and M. Caliez, "Some recent trends in research and technology of advanced thermal barrier coatings", *Aerospace Science and Technology*, Vol.7, 2003, pp.73-80.
[8] J. R. Nicholls and K. J. Lawson, 2002, "Methods to reduce the thermal conductivity of EB-PVD TBC's", *Surface and Coating Technology*, Vols.151-152, 2002, pp.383-391.
[9] S. Alperine, US Patent, 6,333,118 B1, Dec. 2001.
[10] S. Raghavan, H. Wang, W.D. Porter, R.B. Dinwiddie and M.J. Mayo, "Thermal properties of zirconia co-doped with trivalent and pentavalent oxides", *Acta Mater.*, 2000, Vol.49, pp.169-179.
[11] B. Leclercq and R. Mevrel, "Thermal conductivity of zirconia-based ceramics for thermal barrier coatings", in Proceedings, CIMTEC 2002, Firenze, Italy, 2002, p. 365-372.

[12] W. Parker, R. Jenkins, C. Butler, G. L. Abbott, "Flash method of determining thermal diffusivity, heat capacity, and thermal conductivity", *Journal of Applied Physics*, Vol.32, Iss. 9, 1961, pp.1679-1684.

[13] A. Houlbert, P. Cielo, C. Moreau, M. Lamontagne, "Measurement of thermal diffusivity and anisotropy of plasma-sprayed coatings", *International Journal of Thermophysics*, Vol.15, 1994, pp.525-546.

[14] ASTM C373-88, "Standard test method for water absorption, bulk density, apparent porosity, and apparent specific gravity of fired whiteware products", ASTM International: West Conshohocken, 1999.

[15] P. G. Klemens, "Thermal conductivity of inhomogeneous media", *High-Temperature, High-Pressure*, Vol. 23(3), 1991, pp. 241-248.

[16] J. Petitjean, X. Huang and R. Kearsey, "Fracture toughness (K_{IC}) analysis of co-doped 7YSZ", *Materials Science and Technology*, in press, 2010.